Naval Research Laboratory

Washington, DC 20375-5000 NRL Memorandum Report 5886 November 21, 1986

Radiation Transport in a Nitrogen Plasma General Formalism and 1-Dimensional Model

R. D. TAYLOR* AND A. W. ALI

Plasma Physics Division

**Berkeley Research Associates*
Springfield, VA 22150

This work was sponsored by the Defense Advanced Research Projects Agency under ARPA Order 4395, Amendment No. 63 and monitored by the Naval Surface Weapons Center under Contract No. N60921-86-WR-W0233.

SECURITY CLASSIFICATION OF THIS PAGE

REPORT DOCUMENTATION PAGE

1a. REPORT SECURITY CLASSIFICATION UNCLASSIFIED	1b. RESTRICTIVE MARKINGS
2a. SECURITY CLASSIFICATION AUTHORITY	3. DISTRIBUTION / AVAILABILITY OF REPORT Approved for public release; distribution unlimited.
2b. DECLASSIFICATION / DOWNGRADING SCHEDULE	
4. PERFORMING ORGANIZATION REPORT NUMBER(S) NRL Memorandum Report 5886	5. MONITORING ORGANIZATION REPORT NUMBER(S)
6a. NAME OF PERFORMING ORGANIZATION Naval Research Laboratory 6b. OFFICE SYMBOL (If applicable) Code 4700.1	7a. NAME OF MONITORING ORGANIZATION Naval Surface Weapons Center
6c. ADDRESS (City, State, and ZIP Code) Washington, DC 20375-5000	7b. ADDRESS (City, State, and ZIP Code) Silver Spring, MD 20903-5000
8a. NAME OF FUNDING / SPONSORING ORGANIZATION DARPA 8b. OFFICE SYMBOL (If applicable)	9. PROCUREMENT INSTRUMENT IDENTIFICATION NUMBER
8c. ADDRESS (City, State, and ZIP Code) Arlington, VA 22209	10. SOURCE OF FUNDING NUMBERS PROGRAM ELEMENT NO. 62707E; PROJECT NO.; TASK NO.; WORK UNIT ACCESSION NO. DN680-415

11. TITLE (Include Security Classification)

Radiation Transport in a Nitrogen Plasma – General Formalism and 1-Dimensional Model

12. PERSONAL AUTHOR(S)
Taylor, R. D.* and Ali, A. W.

13a. TYPE OF REPORT	13b. TIME COVERED	14. DATE OF REPORT (Year, Month, Day)	15. PAGE COUNT
Interim	FROM _____ TO _____	1986 November 21	41

16. SUPPLEMENTARY NOTATION

*Berkeley Research Associates, Springfield, VA 22150

(Continues)

17. COSATI CODES		
FIELD	GROUP	SUB-GROUP

18. SUBJECT TERMS (Continue on reverse if necessary and identify by block number)

Time dependent; Radiative transfer; Nitrogen plasma; Intense electron beams

19. ABSTRACT (Continue on reverse if necessary and identify by block number)

A time-dependent, multi-line radiative transfer model is developed for a hot nitrogen plasma. The approach relies on a probablistic treatment for propagating photons. While spectral line transfer is emphasized continuum radiation is also accounted for. The model is valid for nonequilibrium conditions. As a first application, the approach is used to describe 1-dimensional transport in two model problems.

Keywords:

20. DISTRIBUTION / AVAILABILITY OF ABSTRACT	21. ABSTRACT SECURITY CLASSIFICATION
☒ UNCLASSIFIED/UNLIMITED ☐ SAME AS RPT. ☐ DTIC USERS	UNCLASSIFIED
22a. NAME OF RESPONSIBLE INDIVIDUAL A. W. Ali	22b. TELEPHONE (Include Area Code) (202) 767-3762 22c. OFFICE SYMBOL Code 4700.1

DD FORM 1473, 84 MAR 83 APR edition may be used until exhausted. All other editions are obsolete.

SECURITY CLASSIFICATION OF THIS PAGE

16. SUPPLEMENTARY NOTATION (Continued)

This work was sponsored by the Defense Advanced Research Projects Agency under ARPA Order 4395, Amendment No. 63 and monitored by the Naval Surface Weapons Center under Contract No. N60921-86-WR-W0233.

CONTENTS

RADIATION TRANSPORT IN A NITROGEN PLASMA GENERAL FORMALISM AND 1-DIMENSIONAL MODEL

I. INTRODUCTION

An energetic electron beam propagating through air dissociates and ionizes N_2 and O_2 leaving behind a hot plasma composed primarily of N, N^+, N^{++}, O, O^+, and O^{++}. Emissions from this plasma cool the heated channel as well as provide diagnostic information. To properly describe the evolution of the channel under nonequilibrium conditions one must solve, simultaneously, the time-dependent rate equations which provide the population densities of all bound and continuum states involved in the radiative and collisional processes and the corresponding radiative transfer equations which account for the effect of the important emissions on the plasma. In this paper we show the effect of radiation transport on the cooling of a nitrogen plasma. The nitrogen plasma consists of N, N^+, and N^{++}, each of which exists in various excited states as well as ground states. The radiation transport is treated as 1-dimensional.

Depending on the nature of the specific problem, there are many approaches to solving the radiative transfer equation[1]. For example, geometry, time-dependence, radiation characteristics (line versus continuum radiation, single lines versus many lines, etc.), optical thickness, inclusion of scattering, and the thermodynamic state of the gas all play a role in determining the best approach and corresponding set of approximations. For instance, rarely is an exact solution attempted for geometries other than planar[2]. In many cases decomposition of the radiative transfer equation into a set of moment equations with corresponding restrictions on the angular dependence of the

Manuscript approved September 3, 1986.

intensity[3] has proven to be a useful procedure. Kulander[4] used such an approach to investigate radiative transfer in a high-temperature nonequilibrium nitrogen plasma confined to a planar geometry. For radiative transfer in optically thick regions, i.e. regions which are large compared to the optical depth of the radiation, the diffusion approximation method, as developed in neutron transport theory[5], may be applicable. Comparisons between moment method, diffusion method, and exact (or nearly exact) results have been made for model problems[6]. Multi-frequency grouping methods are often applied when it is necessary to transport many frequencies and possible to define groups of frequencies within which the absorption coefficients are similiar. Average radiative transfer quantities are then calculated[7]. Combinations of the above approaches may be undertaken as well[8]. One method that has seen extended use is the escape probability formalism, as based on the approach first introduced by Holstein[9]. This method has been used for a variety of problems[10,11].

The approach presented in this paper derives from the escape probability formalism. Spectral line transfer is emphasized. The basic assumption of the theory, therefore, is the absence of correlation between the frequencies of emitted and absorbed photons in the sequential process. This is rigorously satisfied when the line broadening is determined by impact mechanisms as opposed to the Doppler effect. Rather than attempting to solve the transfer equation frequency-by-frequency over a line-width, an effective probability is derived for the propagation of any photon whose origin is a single transition. This approach allows for the treatment of many lines and accounts for the phenomenon that photons emitted from line wings have longer absorption lengths than those emitted near line center. It also provides for a description of such well-known radiative transfer effects as channel cooling due to radiative emission, diffusion of radiation energy, and photo-pumping, i.e. photoabsorption leading to an enhanced production of electrons, ions, and excited atoms/ions. The method is valid for nonequilibrium conditions and when expected reduces to equilibrium results.

The details of the above approach and its relationship to solving the chemistry rate equations are discussed in section II. Specifics of the model, in particular, line profile, geometry, plasma composition, and temperature and energy equations are presented in section III. Numerical results for two models with specific initial conditions given and discussed in section IV. Concluding remarks are reserved for section V.

II. GENERAL FORMALISM

A. Population Dynamics

The coupled rate equations which describe the evolution of the nitrogen plasma include the following collisional and radiative processes: electron impact excitation and de-excitation of N and N^+, electron impact ionization of N and N^+, three-body recombination of N^+ and N^{++}, radiative recombination of N^+ and N^{++}, spontaneous emission, stimulated emission, and absorption for N and N^+. The rate equation for $N_m^{z-1}(r,t)$, i.e. the population density of the (z-1) ion (or neutral if z=1) in the electronic state whose index is m, is

$$
\begin{aligned}
\frac{dN_m^{z-1}}{dt}(r,t) = {} & Ne \left[\sum_{l \le m-1} N_l^{z-1} X_{lm}^{z-1} - N_m^{z-1} \sum_{l \le m-1} Y_{ml}^{z-1} \right] \\
& + Ne \left[\sum_{n \ge m+1} N_n^{z-1} Y_{nm}^{z-1} - N_m^{z-1} \sum_{n \ge m+1} X_{mn}^{z-1} \right] \\
& + Ne \left[Ne \sum_n N_n^z \alpha_{3,nm}^{z-1} + \sum_n N_n^z \alpha_{r,nm}^{z-1} \right] \\
& - Ne \left[Ne\, N_m^{z-1} \sum_l \alpha_{3,ml}^{z-2} + N_m^{z-1} \sum_l \alpha_{r,ml}^{z-2} \right] \\
& - Ne\, N_m^{z-1} \sum_n S_{mn}^{z-1} + Ne \sum_l N_l^{z-2} S_{lm}^{z-2} \\
& + \sum_{n \ge m+1} N_m^{z-1} A_{mn}^{z-1} - N_m^{z-1} \sum_{l \le m-1} A_{ml}^{z-1} \\
& + \sum_{l \le m-1} N_l^{z-1} 4\pi B_{lm}^{z-1} \left[\int_{\Delta\nu_{ml}} J_\nu \phi_\nu \, d\nu \right] \\
& - N_m^{z-1} \sum_{l \le m-1} 4\pi B_{ml}^{z-1} \left[\int_{\Delta\nu_{ml}} J_\nu \chi_\nu \, d\nu \right] \\
& - N_m^{z-1} \sum_{n \ge m+1} 4\pi B_{mn}^{z-1} \left[\int_{\Delta\nu_{nm}} J_\nu \phi_\nu \, d\nu \right] \\
& + \sum_{n \ge m+1} N_n^{z-1} 4\pi B_{nm}^{z-1} \left[\int_{\Delta\nu_{nm}} J_\nu \chi_\nu \, d\nu \right] . \qquad (1)
\end{aligned}
$$

In Eq. (1) all atom, ion, and electron population densities are implicit functions of r and t. The rate coefficients for excitation, de-excitation, ionization, three-body recombination, radiative recombination, and spontaneous emission are designated by X, Y, S, α_3, α_r, and A, respectively. Subscripts refer to the states involved in the particular transition while superscripts identify the ion stage. For example, X_{lm}^{z-1} is the rate coefficient for collisional excitation of ions with net charge z-1 to an electronic state m from state l. The effects of radiation transport on individual species are contained in the last four terms which account for stimulated emission and photoabsorption. These terms depend on the normalized frequency profiles for absorption and emission, ϕ_ν and χ_ν, the appropriate Einstein B-coefficient, the linewidths $\Delta\nu$, and the mean angle-averaged intensity, $J_\nu(r,t)$. The mean intensity J_ν is obtained by solving the radiative transfer equation for frequency ν; this is discussed in detail later below.

The radiation terms in Eq. (1) are simplified by assuming the emission and absorption profiles are identical. Using the standard relations between the Einstein coefficients Eq. (1) becomes

$$\frac{dN_m^{z-1}}{dt}(r,t) = \text{collisional terms} + \text{spontaneous emission}$$

$$+ \sum_{l \le m-1} \frac{c^2}{2h\nu_{ml}^3} \left[\int_{\Delta\nu_{ml}} J_\nu \, \phi_\nu \, d\nu \right] N_m^{z-1} A_{ml}^{z-1} \left[\frac{g_m^{z-1}}{g_l^{z-1}} \frac{N_l^{z-1}}{N_m^{z-1}} - 1 \right]$$

$$- \sum_{n \ge m+1} \frac{c^2}{2h\nu_{nm}^3} \left[\int_{\Delta\nu_{nm}} J_\nu \, \phi_\nu \, d\nu \right] N_n^{z-1} A_{nm}^{z-1} \left[\frac{g_n^{z-1}}{g_m^{z-1}} \frac{N_m^{z-1}}{N_n^{z-1}} - 1 \right] . \quad (2)$$

Stimulated emission is now treated as a modification to absorption.

If, in Eq. (2), a "gross re-absorption factor" is defined for each transition line as

$$1 - \Lambda_{ml}^{z-1} = \frac{c^2}{2h\nu_{ml}^3} \left[\int_{\Delta\nu_{ml}} J_\nu \, \phi_\nu \, d\nu \right] \left[\frac{g_m^{z-1}}{g_l^{z-1}} \frac{N_l^{z-1}}{N_m^{z-1}} - 1 \right] \quad (3)$$

then the rate equation becomes

$$\frac{dN_m^{z-1}}{dt}(r,t) = \text{collisional terms + spontaneous emission}$$

$$+ \sum_{l \leq m-1} N_m^{z-1} (1 - \Lambda_{ml}^{z-1}) A_{ml}^{z-1}$$

$$- \sum_{n \geq m+1} N_n^{z-1} (1 - \Lambda_{nm}^{z-1}) A_{nm}^{z-1} \quad . \quad (4)$$

Optically thick and thin results are frequently obtained by treating the set of $\{\Lambda\}$ as constants with values ranging between 0 and 1. In this manner the radiative transfer equation need not be solved and limiting population densities are obtained[12-16].

B. Radiative Transfer Equation

The radiative transfer equation in its simplest form is

$$\frac{dI_\nu}{ds} = - \kappa'_\nu I_\nu + j_\nu \quad . \quad (5)$$

Here, κ'_ν is the absorption coefficient (corrected for stimulated emission) at frequency ν, j_ν the emission coefficient for the radiation, I_ν the intensity, and s defines a ray through the medium. The general non steady-state solution to Eq. (5) is written in integral form as

$$I_\nu(r,t,\Theta,\Psi) = \int_{s_o}^{s} ds' \, j_\nu(s',t') \, e^{-\int_{s'}^{s} \kappa'_\nu(s'',t'') \, ds''} \quad . \quad (6)$$

In Eq. (6) $t' = t-(s-s')/c$, $t'' = t-(s-s'')/c$, and $j_\nu\, ds'$ is the amount of radiation born at s',t' on ray ds' in a direction Θ,Ψ. Multiplying by the exponential gives the fraction of radiation that arrives at s,t. The coordinate system is shown in Fig. 1. In this study continuum absorption and emission are neglected. The emission coefficient for a specific transition line ν_{ml} is

$$j_\nu = \frac{h\nu_{ml}}{4\pi} A_{ml}^{z-1} \phi_\nu N_m^{z-1} \tag{7}$$

The absorption coefficient for the same transition is

$$\kappa'_\nu = \kappa_\nu \left[1 - \frac{g_l^{z-1} N_m^{z-1}}{g_m^{z-1} N_l^{z-1}} \right] \tag{8}$$

where

$$\kappa_\nu = -\frac{\lambda_{ml}^2}{8\pi} \frac{g_m^{z-1}}{g_l^{z-1}} N_l^{z-1} A_{ml}^{z-1} \phi_\nu \quad . \tag{9}$$

The statistical weights for the upper and lower states are g_m^{z-1} and g_l^{z-1}.

It is the mean intensity $J_\nu(r,t)$ that enters into Eq. (2) and determines the effect of radiation transport on the individual population densities. Letting $\rho = |r - r'|$, defining the volume element $dV = dr' = \rho'^2 \sin\Theta\, d\Theta\, d\Psi\, d\rho'$, and averaging over Θ,Ψ the mean intensity is

$$J_\nu(r,t) = \frac{h\nu_{ml}}{4\pi} A_{ml}^{z-1} \phi_\nu \int_0^{\rho_m} dr' \frac{N_m^{z-1}(r',t')}{4\pi\, \rho'^2} e^{-\int_0^{\rho'} \kappa'_\nu(r'',t'')\, d\rho''} \tag{10}$$

where $t' = t-\rho'/c$ and $t'' = t-\rho''/c$. Eq. (10) gives the angle-averaged solution to the radiative transfer equation for a specific frequency ν.

C. Population Dynamics Plus Radiative Transfer

The rate equations may be rewritten in simpler form as

$$\frac{dN_m^{z-1}}{dt}(r,t) = \text{collisional terms + spontaneous emission} + \sum_{l \leq m-1} R_{ml}^{z-1} A_{ml}^{z-1} - \sum_{n \geq m+1} R_{nm}^{z-1} A_{nm}^{z-1} \qquad (11)$$

where the set {R} is defined by comparison with Eq. (2). Substituting Eq. (10) into the absorption term, noting that κ'_ν is given by Eq. (8), and interchanging the ν and r' integrations results in

$$R_{ml}^{z-1}(r,t) = \int dr' \; N_m^{z-1}(r',t') \; G_{ml}(r',t';r,t) \quad . \qquad (12)$$

G_{ml} is the probabilty that a photon emitted at r',t' is absorbed in a volume element dr at r,t and is given as

$$G_{ml}(r',t',r,t) = \frac{1}{4\pi \, |r-r'|^2} \int_{\Delta\nu_{ml}} d\nu \; \phi_\nu \; \kappa'_\nu(r,t) \; e^{-\int_0^{\rho'} d\rho'' \; \kappa'_\nu(r'',t'')} \quad . \qquad (13)$$

The discretized version of Eqs. (11) - (13) forms the basis for the "escape-probability formalism" discussed previously.

It is useful to compare G_{ml} to $T_{ml}(\rho';t)$, i.e. the probability a photon travels a distance ρ' without being absorbed, defined as

$$T_{ml}(\rho';t) = \int_{\Delta\nu_{ml}} d\nu \; \phi_\nu \; e^{-\int_0^{\rho'} d\rho'' \; \kappa'_\nu(r'',t-\rho''/c)} \quad . \qquad (14)$$

Specifically, if $\kappa'_\nu(r,t) = \kappa'_\nu(r',t')$ then the following relation holds,

$$G_{ml}(r',t';r,t) = \frac{-1}{4\pi\ \rho'^2} \frac{\partial}{\partial \rho'} T_{ml}(\rho';t) \quad . \qquad (15)$$

Physically, the requirement is that over the mean free path of an emitted photon the absorption coefficient does not change much, i.e. the number of absorbers encountered during transit remains nearly constant. $T_{ml}(\rho';t)$ can be written as

$$T_{ml}(\rho',t) = \int_{\Delta\nu_{ml}} d\nu\ \phi_\nu\ e^{-\kappa'_\nu(r,t)\ \rho'} \qquad (16)$$

Eq. (16) was initially introduced by Holstein[9] and evaluated for various line profiles.

The problem is now reduced to the following steps: (1) For the transitions included in the model choose an appropriate line shape and evaluate Eq. (16) either exactly or approximately. (2) For the desired geometry obtain the set {G} from Eq. (15). (3) Use these to evaluate the absorption terms in Eq. (12). (4) Solve the rate equations. The procedure must be done self-consistently since κ_ν' depends on the solution to the rate equations.

III. MODEL

A. Nitrogen Plasma

Our interest is in studying radiative transfer in a hot channel, in particular, for electron temperatures of 1.0 - 3.0 eV. In this temperature range the constituents are primarily atomic or ionic. We have included in the calculations the lowest 13 levels of N, the lowest 17 levels of N^+, and 2 representative levels of N^{++}. Details of the model have been presented elsewhere[13,14]. All bound-bound radiative transitions allowed by this energy scheme are included and form the basis for the line radiation discussed previously. In this manner the dominant uv and visible spectral lines are transferred.

B. T(ρ)

The absorption coefficients, defined in Eqs. (8) and (9), depend on the line shape, ϕ_ν. We have assumed this line shape is given by a Lorentzian, i.e.

$$\phi_{\nu,ml} = \frac{1}{\pi} \frac{\Delta\nu}{(\nu - \nu_{ml})^2 + (\Delta\nu)^2} \quad . \tag{17}$$

The line width is $\Delta\nu$. In the temperature and electron density regimes of interest, Ne ≈ [10^{16} - 10^{19} cm^{-3}], Doppler and Stark broadening are the two dominant mechanisms. The Lorentz profile, Eq. (17), is characteristic of the Stark broadening, where isolated spectral lines of atoms in dense plasmas are broadened by electron impact[17]. However, in our computations we consider the effects of both Doppler and Stark broadening whose actual line shape should be a Voight profile. In the computations described below, we calculate the line broadening of both as a function of frequency, electron temperature, and electron density and choose $\Delta\nu$ to be the greater of the two. The Stark effect generally dominates. Additional details have been presented elsewhere[18].

For the Lorentzian line shape Holstein[9] obtained the asymptotic functional form of Eq. (16) as

$$T_{ml}(\rho) \simeq \frac{1}{(\pi\kappa_{ml}\rho)^{1/2}} \qquad \kappa_{ml}\rho >> 1 \quad . \tag{18}$$

κ_{ml} is the absorption coefficient at line center. The exact integration of $T(\rho)$ is shown in Fig. 2 along with two empirical approximations. For $x = \kappa_{ml}\rho$ the dotted line corresponds to

$$T_{ml}(\rho) = e^{-x} + \frac{\left[\, 1 - e^{-.8x^{3/2}} \,\right]}{(\pi x)^{1/2}} \tag{19}$$

while the dashed line corresponds to

$$\begin{aligned} T_{ml}(\rho) &= 1 - x/3 && x \leq 1 \\ &= (2/3)\, x^{-1/2} && x \geq 1 \quad . \end{aligned} \tag{20}$$

Eq. (20) is used in this study.

C. Geometry and G_{ml}

The results discussed in section IV are for a geometry where radiation is assumed to flow in only two directions, but along one dimension, i.e. $r = r$. The plasma is contained within a finite region, $-L \leq r \leq L$, so in addition to transfer, energy is radiated beyond the boundary. For this geometry the $4\pi\rho'^2$ factor in Eq. (15) is excluded.

When evaluating Eq. (12) care must be taken to properly consider three possible cases which depend on the absorption length at line center, κ_{ml}, and the distance to the boundary edge, L. The radiation may be thick in both directions, $L-r \geq 1/\kappa_{ml}$ and $L+r \geq 1/\kappa_{ml}$. It may be thin in both directions, $L-r \leq 1/\kappa_{ml}$ and $L+r \leq 1/\kappa_{ml}$, or thick in one direction and thin in the other, $L+x \geq 1/\kappa_{ml}$ and

$L-x \geq 1/\kappa_{ml}$. Symmetry considerations enable us to reduce computations to the half space r = [0,L]. A typical absorption term for the case where the line is thick in each direction is

$$R_{ml}^{z-1}(r,t) = \frac{\kappa_{ml}}{6} \int_0^{1/\kappa_{ml}} d\rho \; N_m^{z-1}(\rho,t)$$

$$+ \frac{1}{6\,\kappa_{ml}^{1/2}} \int_{1/\kappa_{ml}}^{\rho_m} d\rho \; \frac{N_m^{z-1}(\rho,t)}{\rho^{3/2}}$$

$$+ \quad \text{contribution from the left} \quad . \qquad (21)$$

Note that $\kappa_{ml} = \kappa_{ml}(r,t)$ and $\rho_m = L-r$. Similiar results are obtained for the other cases.

D. Temperature Equation

As radiation is transferred from one local region within the plasma to another, cooling or heating may take place. As radiation escapes the plasma entirely, a net cooling occurs. To model this phenomenon the relevant temperatures, generally, electron and gas, must be monitored. For hot channels created by intense electron beams the plasma electron temperature and the gas kinetic temperature frequently reach an identical value, afterwhich the subsequent evolution is well described by a single temperature. In the present model it is assumed that for a given set of initial conditions the plasma is characterized by a single temperature, i.e. $T(r,t) = Te(r,t) = Tg(r,t)$. The time evolution of T(r,t) is obtained from the energy conservation equation,

$$\frac{3}{2}\, T(r,t) \left(Ne(r,t) + Ng(r,t) \right) = E_p(r,0) + E_g(r,0) +$$

$$E_c(r,0) - Erad(r,t) - E_c(r,t) \; . \qquad (22)$$

Here, $E_p(r,0)$, $E_g(r,0)$, and $E_c(r,0)$ are the plasma, gas kinetic, and chemical energies at t = 0 for point r, respectively. Ne(r,t) and Ng(r,t) are the electron and total gas particle densities at time t and point r. $E_c(r,t)$ is the chemical energy at time t and Erad(r,t) is the amount of energy radiated from (or to if Erad < 0) point r at time t. Erad(r,t) is obtained by solving the following equation,

$$\frac{d}{dt}\,\mathrm{Erad}(r,t) = \sum_{m,l,z} \left[R_{ml}^{z-1}(r,t) - N_{ml}^{z-1}(r,t) \right] A_{ml}^{z-1}\, h\nu_{ml} + \text{continuum radiation} . \qquad (23)$$

Continuum radiation results from free-free and free-bound (radiative recombination) transitions. In this model radiation from free-free transitions is neglected, uv radiation from all 2-body recombination events is assumed to be optically thick while visible radiation from these events is optically thin. Eqs. (11), (22), and (23) are the essence of the model. The detailed radiative transfer is contained in Eqs. (11) and (23). Eq.(22) insures energy conservation.

IV. NUMERICAL RESULTS

Numerical integration of Eqs. (11) and (23) is accomplished by using CHEMEQ, a routine designed to solve stiff ordinary differential equations[19]. Symmetry enables us to carry out the integration over half the grid, i.e. [0,L]. In this section the following initial conditions are assumed: The size of the region is 1 cm, i.e. L = .5 cm. Initial population densities are distributed uniformly across the grid [0,L]. The values are $N(1)+N(2)+N(3) = 3.715 \times 10^{19}$ cm^{-3}, $Ne = N^+(1)+N^+(2)+N^+(3) = 5.0 \times 10^{16}$ cm^{-3}, and all others are set to 0.0 (actually, 1×10^4 cm^{-3}). The specific ground N and N^+ states are populated according to statistical weights. Two initial temperature profiles are assumed. The first is a uniform distribution; Te = 3.0 eV for $0.0 \leq r \leq .5$ cm. The second is non-uniform; Te = 3.0 eV for $0.0 \leq r \leq .2$ cm and decreases linearly to a value of 1.5 eV at r = .5 cm. Setting the initial population densities and temperatures is equivalent to setting the initial plasma electron, gas kinetic, and chemical energy distributions.

Eqs. (11) and (23) are integrated until an equilibrium is nearly established. During the integration the radiation terms, for example, Eq. (21), are updated using the solutions to the rate equations. Initially this is done every 10^{-10} sec and relaxed to 10^{-7} sec at longer times. Figs. 3a - 10a correspond to the uniform temperature distribution results, while Figs. 3b - 10b are for the non-uniform case.

A. Rate Equation Results

Figs. 3 and 4 show radiative transfer and cooling as evidenced by the evolution of T(r,t) up to $t = 10^{-5}$ sec for r = 0.0, 0.25, and 0.5 cm. For both cases the species rapidly approach a local equilibrium while the energy in the system readjusts. This occurs because the initial conditions correspond to a nonequilibrium situation. The initial relaxation takes approximately 10 ns during which time radiative transfer has not begun to play a significant role. For the uniform case cooling is nearly constant

across the grid for 10 μsec. The outer boundary does show a lower temperature than the interior, particularly for 5 - 8 μsec. This is due to more energy loss. The non-uniform case shows the center cooling more rapidly than the boundary region. Even at 10 μsec a temperature gradient remains.

Fig. 5 shows the time evolution of the electron density for both cases. While the electron density was initially constant across the grid for the uniform case the extra energy lost from the boundary lead to a decrease in temperature, mentioned above, which in turn lead to a lower Ne at the edge. By contrast Ne at the boundary for the non-uniform case decreases only slightly from its maximum while the interior values decrease more rapidly, reflecting the behavior of T(r,t).

B. Energy Loss Results

The time histories of the energy profiles for r = 0.0 and 0.5 cm are presented in Figs. 6 and 7. In all cases the amount of chemical energy exceeds the gas kinetic energy which is greater than the plasma electron energy. Figs. 6a and 7a show the extent to which more energy is radiated from the boundary than from the center. Since there was less energy at the grid edge than at the center for the non-uniform case, the opposite situation is seen in Figs. 6b and 7b. In terms of energetics these figures show that the time scale for radiative transfer to contribute significant energy loss is on the order of microseconds. The radiative energy loss values, Erad(r,t), for r = 0.0, 0.25, and 0.5 cm are show in Fig. 8. By 10 μsec these terms have nearly saturated as have the energy values.

Throughout the integration the photon energy that is created, re-absorbed, and radiated from the system is monitored. One quantity of interest is the radiated energy flux for each line, Q_{ml}, given in units of eV-cm^{-2}-sec^{-1}. The flux radiating from one side is calculated according to

$$Q_{ml}^{z-1} = \int_0^R dr\ N_m^{z-1}(r,t)\ A_{ml}^{z-1}\ h\nu_{ml} \left[1 - \frac{R_{ml}^{z-1}(r,t)}{N_m^{z-1}(r,t)} \right] . \qquad (24)$$

Table 1 shows the flux values for the major contributing lines as a function of time. The surge in emitted radiation at 1 ns corresponds to the rapid population of exited N and N^+ states during the initial energy redistribution period. Subsequent time behavior shows a slowing down of the cooling rate as radiation energy is lost from the system. Generally, the energy loss is dominated by emissions from the nitrogen uv lines. The N^+ uv lines and N optical lines also contribute to the energy loss, though to a lesser degree; their contribution is not shown. The effect of the N^+ visible lines is negligible. This is consistent with the corresponding temperature values.

TABLE 1

Radiated Energy Flux ($eV\text{-}cm^{-2}\text{-}sec^{-1}$)

Time	Transition Line (Å)					Total
	1493.3	1134.6	1199.9	1743.6	1243.3	
100 ps	7.8×10^{17}	1.0×10^{17}	2.2×10^{17}	3.9×10^{17}	2.3×10^{17}	1.9×10^{18}
1 ns	8.0×10^{23}	6.3×10^{23}	5.7×10^{23}	4.6×10^{23}	1.7×10^{23}	2.8×10^{24}
10 ns	4.4×10^{23}	3.6×10^{23}	3.4×10^{23}	2.6×10^{23}	2.1×10^{23}	2.0×10^{24}
100 ns	3.9×10^{23}	3.6×10^{23}	2.9×10^{23}	2.3×10^{23}	2.0×10^{23}	1.9×10^{24}
1 μs	3.4×10^{23}	2.9×10^{23}	2.5×10^{23}	2.0×10^{23}	1.7×10^{23}	1.6×10^{24}
10 μs	9.2×10^{22}	6.7×10^{22}	6.4×10^{22}	6.2×10^{22}	3.5×10^{22}	3.9×10^{23}

C. Line Results

It is convenient to define a line-integrated mean intensity, J_{ml}^{z-1}, as

$$J_{ml}^{z-1}(r,t) = \int_{\Delta\nu_{ml}} J_{\nu}^{z-1} \phi_{\nu} \, d\nu \quad . \tag{25}$$

In terms of the appropriate absorption term and population densities it follows that

$$J_{ml}^{z-1}(r,t) = \frac{2h\nu_{ml}^3}{c^2} \frac{R_{ml}^{z-1}(r,t)}{N_m^{z-1}(r,t)} \left[\frac{g_m^{z-1} N_l^{z-1}(r,t)}{g_l^{z-1} N_m^{z-1}(r,t)} - 1 \right]^{-1} . \tag{26}$$

Figs. 9 - 10 show the line integrated mean intensities for 2 transition lines (1199.9 Å, and 8211.8 Å) at different times (10 ns, 100 ns, 1μs, and 10μs). The distribution of radiation for these lines is, therefore, monitored as a function of time and space. The results are consistent with the associated temperature profiles. As expected the line intensities for the uniform case show much less variation over the grid than the non-uniform case, particularly at early times. As radiation transfer occurs energy diffuses outward. Fig. 9b, in particular, shows the extent to which the line intensity in the central region decreases compared to the outer region as a function of time.

D. Discussion

Diffusion and cooling are two aspects of the radiative transfer process. When energy is distributed uniformly across a confined region it is seen that the outer boundary cools more rapidly than the interior, thus establishing a temperature (or energy) gradient which drives subsequent transfer and net cooling. Radiative transfer initiated by the existence of a temperature gradient behaves differently.

In this case energy diffuses outward from the outset and the hotter inner region cools more rapidly than the cooler outer region. Using the model descibed previously the above numerical results for the given set of initial conditions demonstrate that the radiative transfer time is on the order of microseconds. This can be understood within the context of the following simple picture:

If radiative transfer is considered to be a sequence of photon emissions and absorptions it should be possible to estimate bounds on the time required for radiation to diffuse from the center of a region to a boundary. For a specific transition line, m→l, the diffusion time may be estimated as

$$t_{ml} = \frac{L}{x_{ml}} \frac{1}{A_{ml}} \tag{27}$$

$$= 1/A^{*}_{ml} \tag{28}$$

where L is the distance to the boundary (.5 cm in this study) and x_{ml} is the "mean free path". This definition corresponds to the following picture: After a photon travels a distance x_{ml} it is absorbed and re-emitted in $1/A_{ml}$ (seconds). It continues on in this manner until reaching the boundary. In Eq. (28) the effective emission coefficient is defined as $A^{*}_{ml} = A_{ml}/\tau_{ml}$ where τ_{ml} is the optical depth.

Within the context of our radiative transfer model, the definition of x_{ml} is not obvious. The simplest choice is to define x_{ml} as the inverse of the absorption coefficient at line center, $x_{ml} = 1/\kappa_{ml}$. This puts the emphasis for radiative transfer on photons that are emitted directly at the center of the frequency profile. The probability that a photon travels this far without being absorbed, as given by Eq. (20), is 0.67. In the simple diffusion picture it is assumed that the photon is then absorbed. This gives an upper bound on the diffusion time scale. For comparison, x_{ml} is defined as the distance at which $\Gamma_{ml}(\rho) = 0.05$. In this manner absorption is guaranteed after the photon has

travelled $x_{ml} = 177.8/\kappa_{ml}$. The later definition places more emphasis for radiative transfer on photons emitted from the line wings since these are the photons that contribute to the asymptotic behavior of $T_{ml}(\rho)$. This gives a lower bound for the onset of radiative transfer.

Table 2 shows a comparison of these diffusion times for the top 12 lines contributing to radiation, as determined by Q_{ml} at t = 10 ns. The diffusion time using $x_{ml} = 1/\kappa_{ml}$ is denoted as t^{1}_{ml} and t^{wing}_{ml} is the estimate for the larger value of x_{ml}. These estimates are in fact consistent with the results presented in Figs. 3 - 10.

TABLE 2

Diffusion Time Estimates (sec)

Wavelength (Å)	$\kappa^{r=0}_{lm}(cm^{-1})$	t^{1}_{ml}	t^{wing}_{ml}
1493.3	7.3×10^{3}	6.6×10^{-6}	3.7×10^{-8}
1134.6	4.6×10^{4}	4.3×10^{-5}	2.4×10^{-7}
1199.9	2.3×10^{4}	4.9×10^{-5}	2.8×10^{-7}
1743.6	2.2×10^{3}	5.5×10^{-6}	3.1×10^{-8}
1243.3	7.7×10^{3}	8.4×10^{-6}	4.7×10^{-8}
1085.1	7.5×10^{3}	6.6×10^{-6}	3.7×10^{-8}
1411.9	4.9×10^{2}	4.9×10^{-6}	2.7×10^{-8}
8617.5	7.0×10^{1}	1.2×10^{-6}	6.6×10^{-9}
9i6.3	9.3×10^{3}	2.6×10^{-6}	1.5×10^{-8}
8617.5	1.6×10^{1}	2.6×10^{-7}	1.5×10^{-9}
7452.2	1.3×10^{1}	2.1×10^{-7}	1.2×10^{-9}
9395.3	2.3×10^{1}	5.7×10^{-7}	3.2×10^{-9}

V. CONCLUDING REMARKS

A radiative tranport model has been developed which emphasizes the transfer of line radiation in a hot nitrogen plasma. The radiative transfer equations are solved self-consistently with the corresponding time-dependent chemistry equations. This approach allows for the transfer of many lines and does not require a state of LTE to exist. Numerical results for two simple test cases show the utility of the model in describing radiative transfer effects. A following report will present the results of using this model to account for radiation transport in the realistic description of a plasma generated by an intense electron beam.

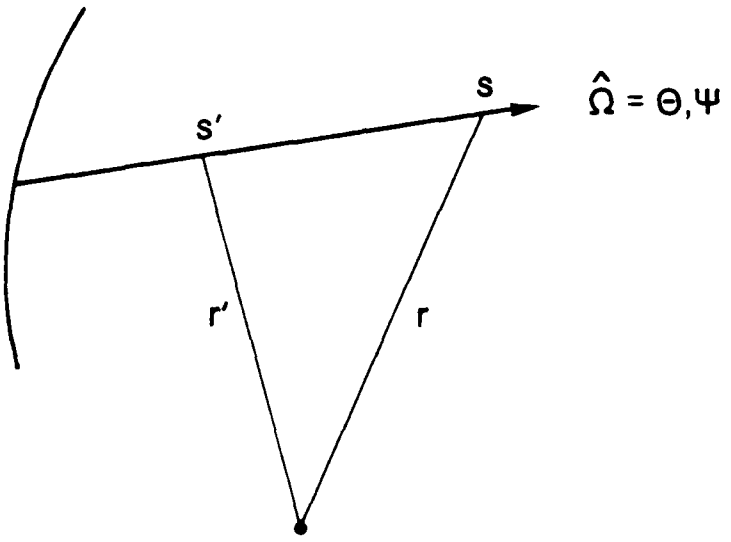

$$\rho' = s - s' = |r - r'|$$

Fig. 1 Coordinate system.

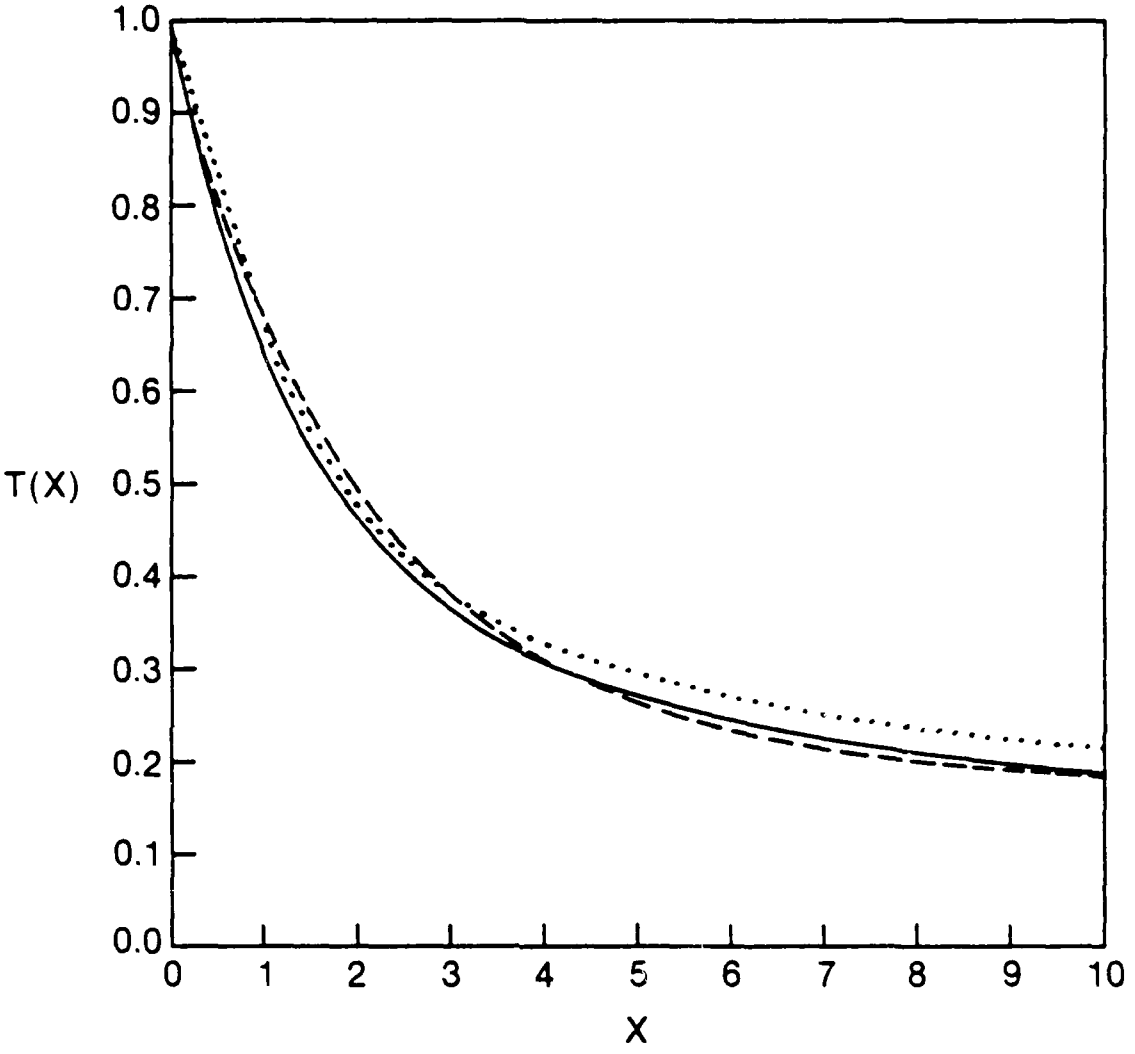

Fig. 2 $T(x=\kappa_{ml}\rho)$. Exact integration is solid line. Eq. (19) is dashed line. Eq. (20) is dotted line.

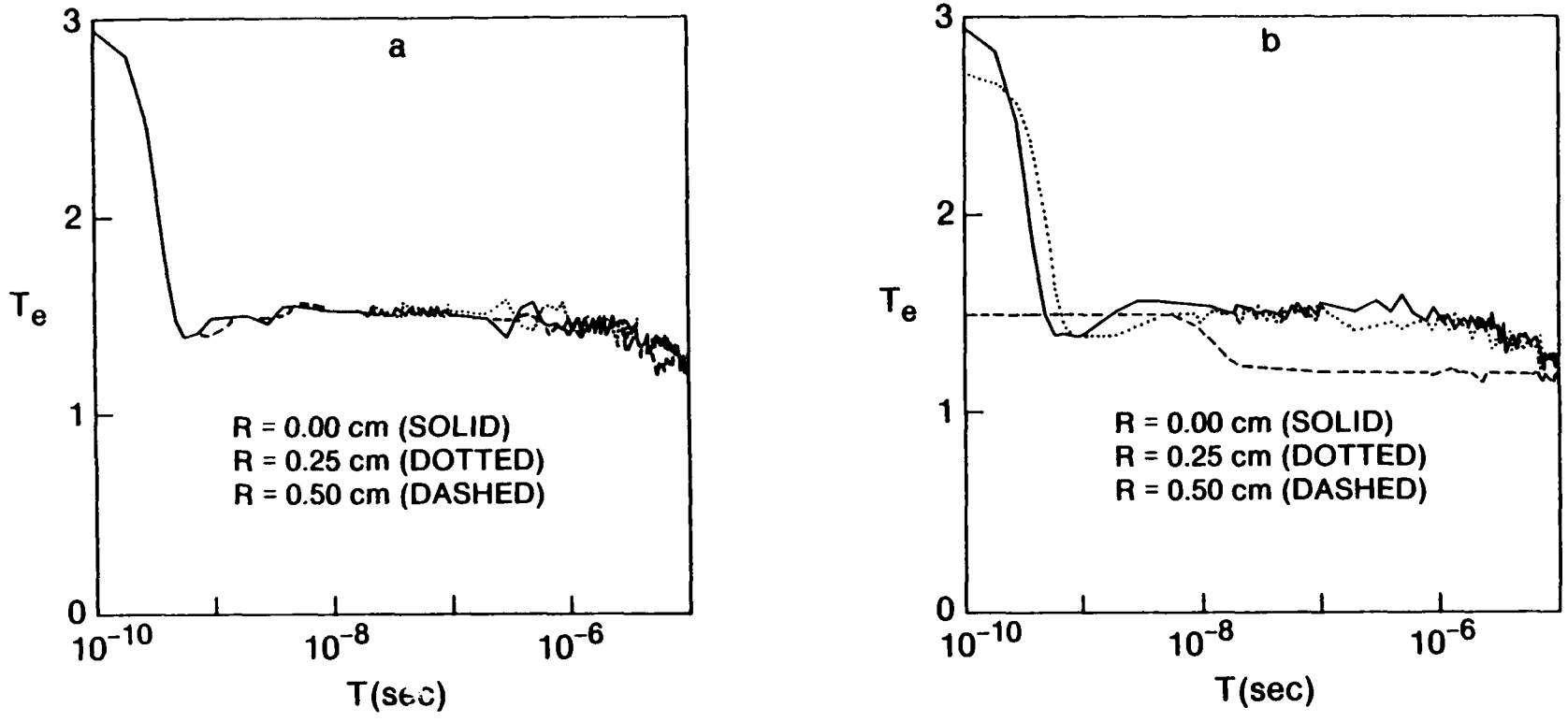

Fig. 3 Temperatures for r = 0.0 cm (solid line), 0.25 cm (dotted line), and 0.5 cm (dashed line). a) Uniform initial conditions. b) Non-uniform initial conditions.

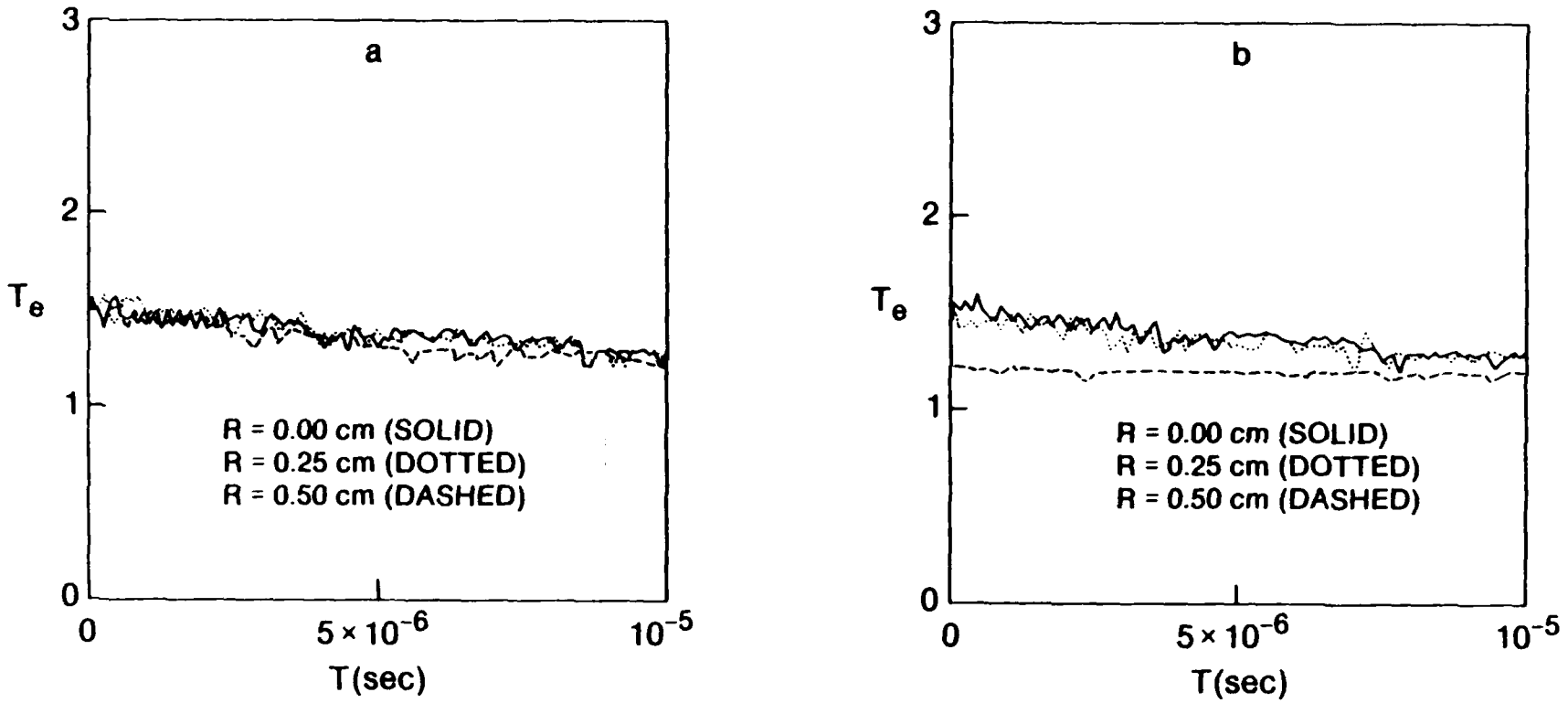

Fig. 4 Same as Fig. 3.

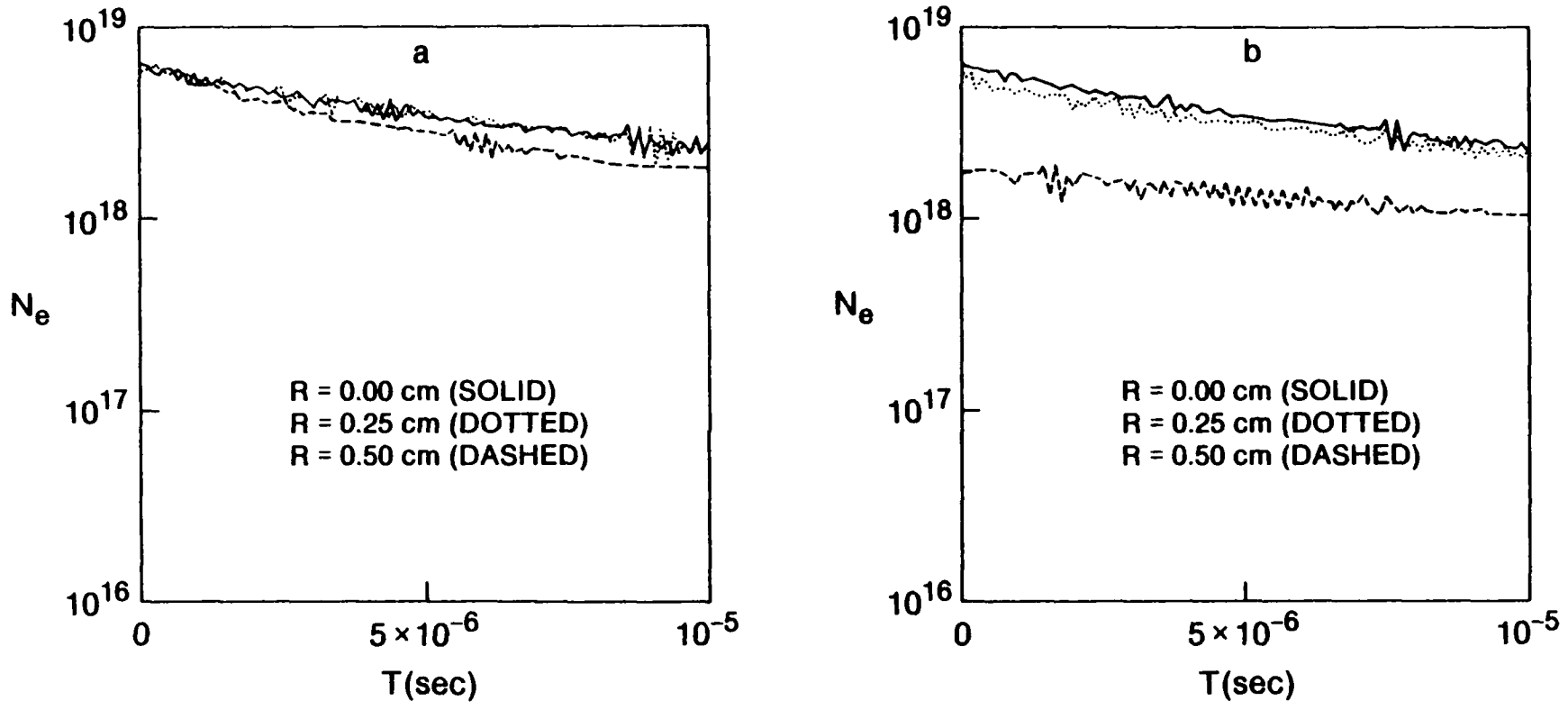

Fig. 5 Electron densities for r = 0.0 cm (solid line), 0.25 cm (dotted line), and 0.5 cm (dashed line). a) Uniform initial conditions. b) Non-uniform initial conditions.

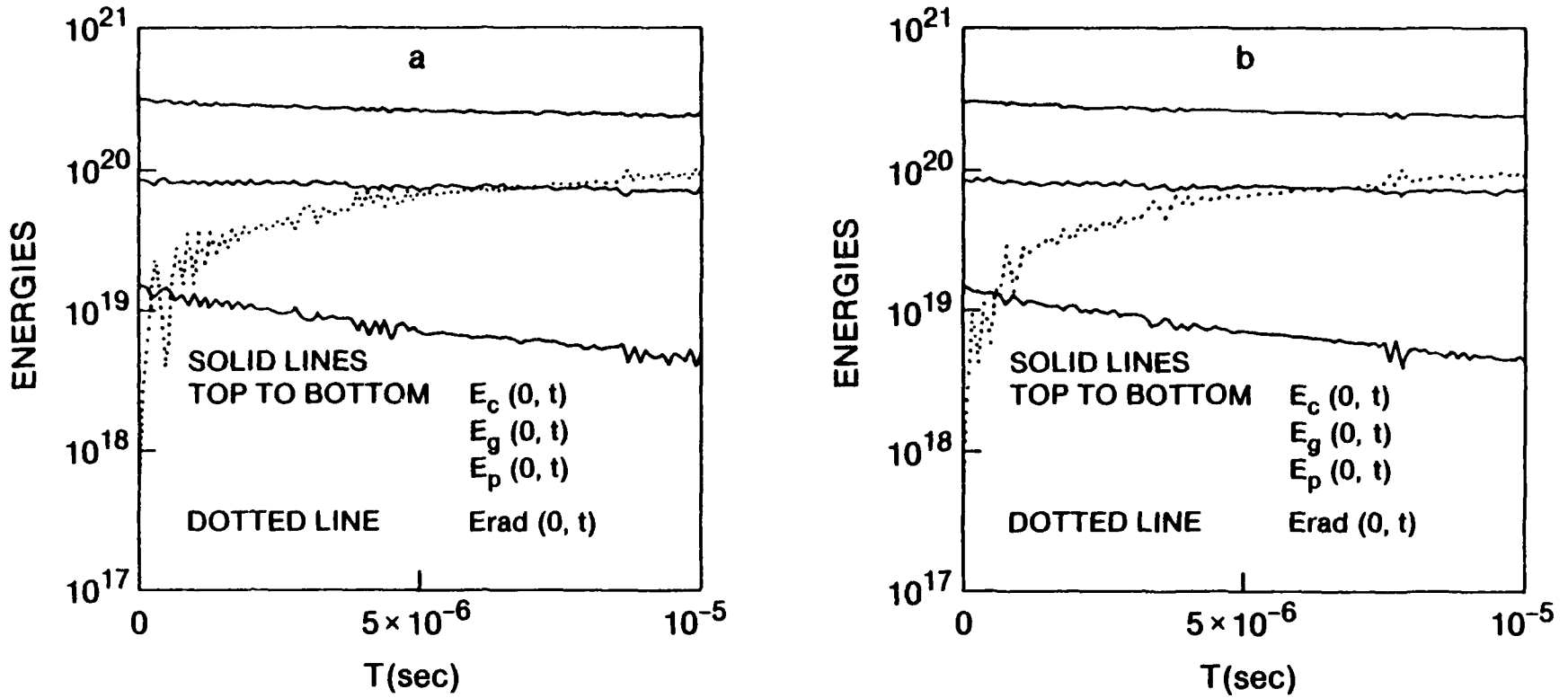

Fig. 6 Chemical (top line), gas kinetic (middle line), plasma electron (bottom line), and radiation energies (dotted line) for r = 0.0 cm. a) Uniform initial conditions. b) Non-uniform initial conditions.

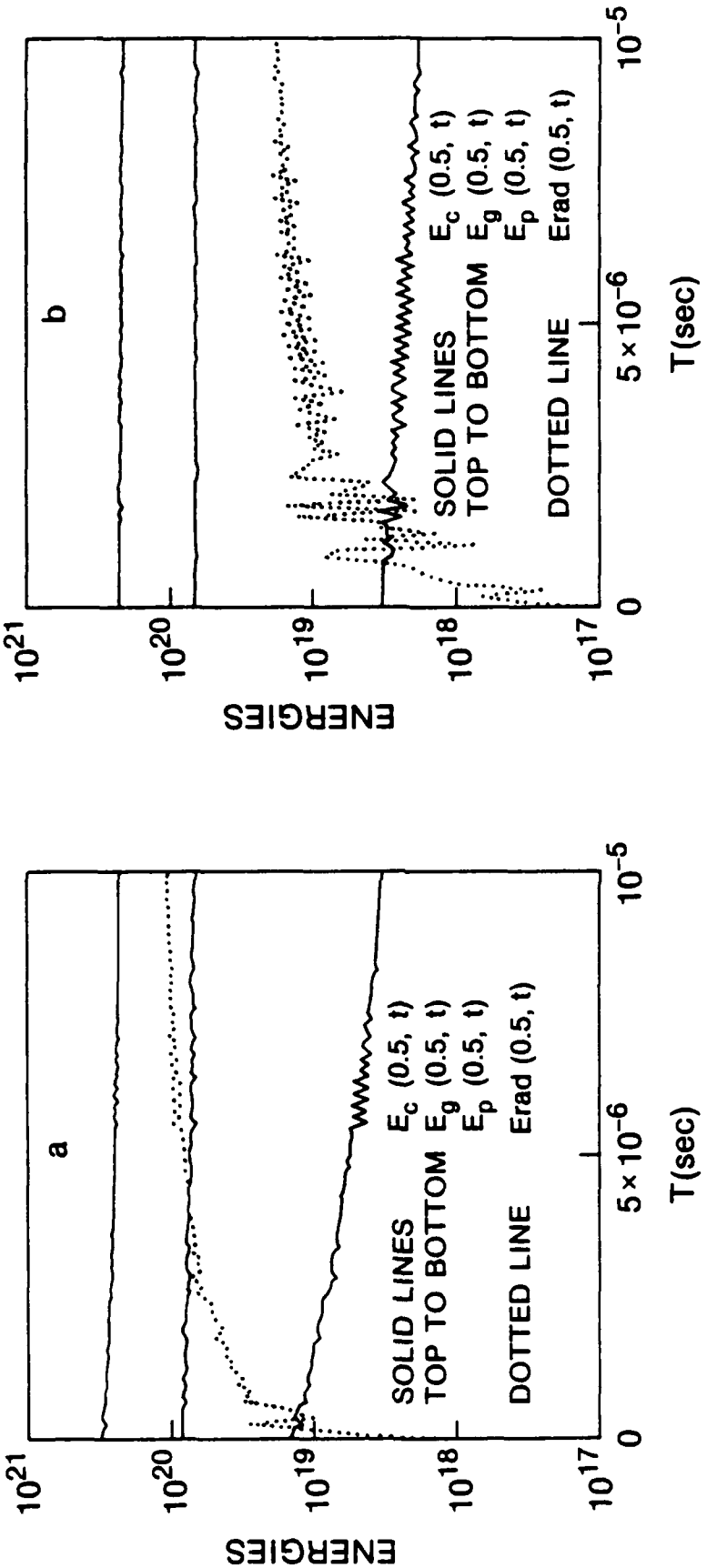

Fig. 7 Same as Fig. 6 for r = 0.5 cm.

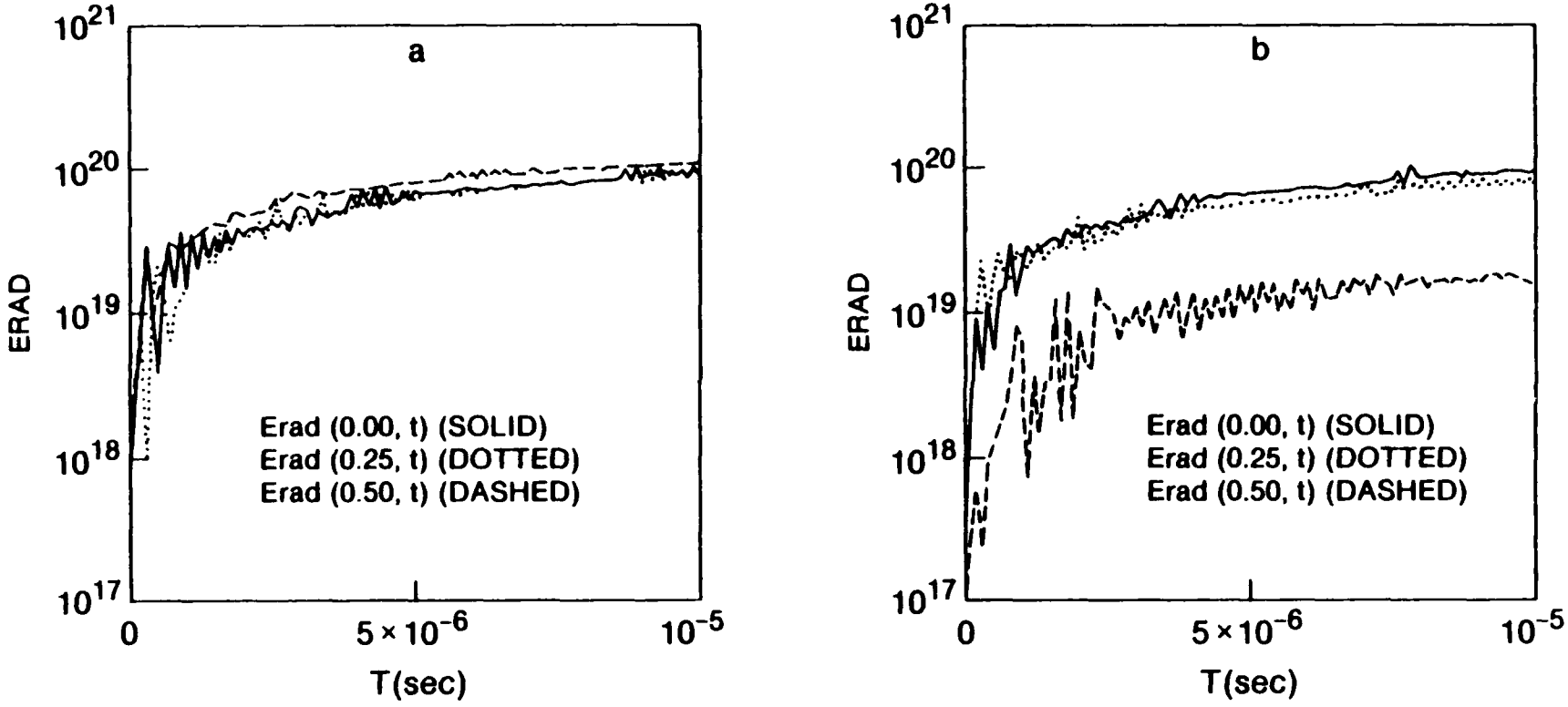

Fig. 8 Radiation energies for r = 0.0 cm (solid line), 0.25 cm (dotted line), and 0.5 cm (dashed line). a) Uniform initial conditions. b) Non-uniform initial conditions.

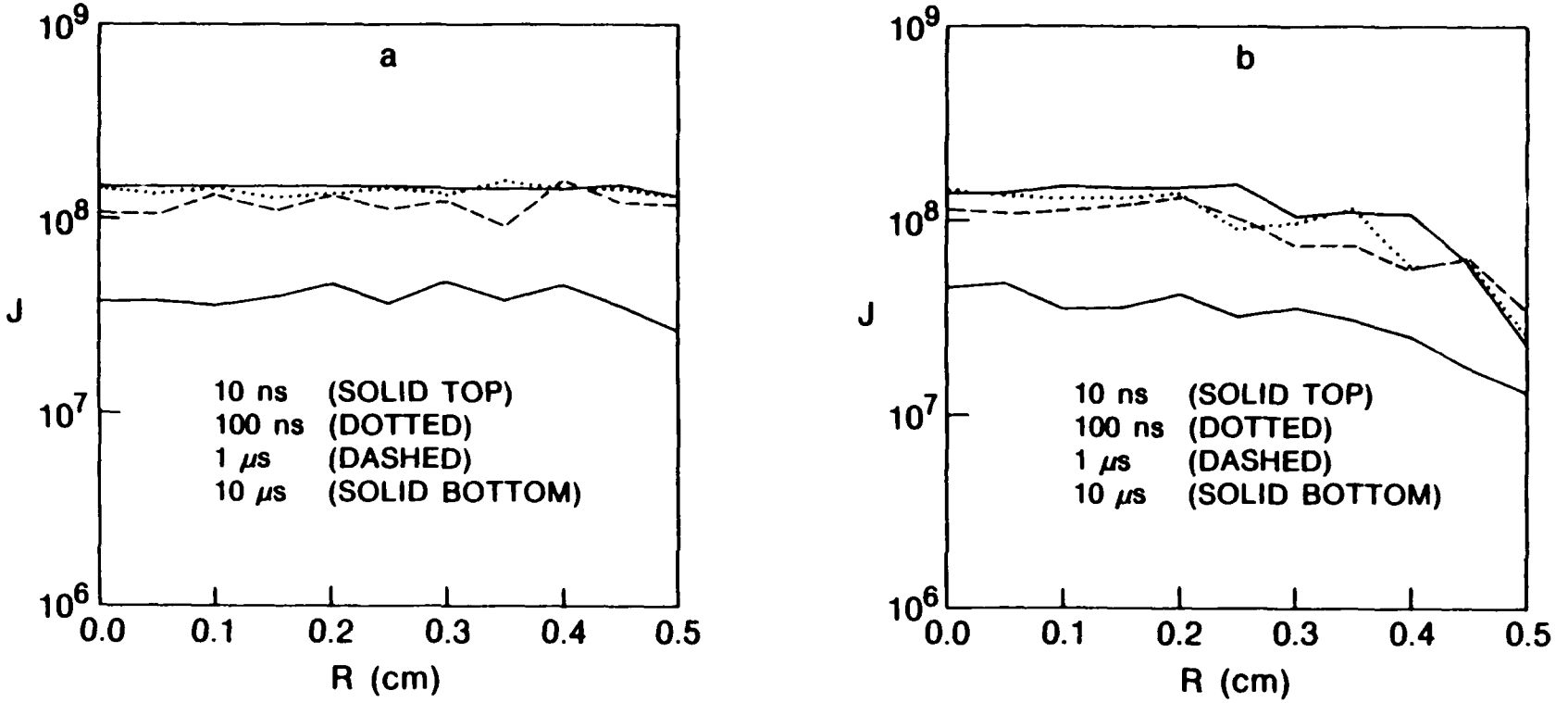

Fig. 9 Line intensities, Eq. (26), for 1199.9 Å line at 10 ns (top solid line), 100 ns (dotted line), 1 μs (dashed line), and 10 μs (bottom solid line). a) Uniform initial conditions. b) Non-uniform initial conditions.

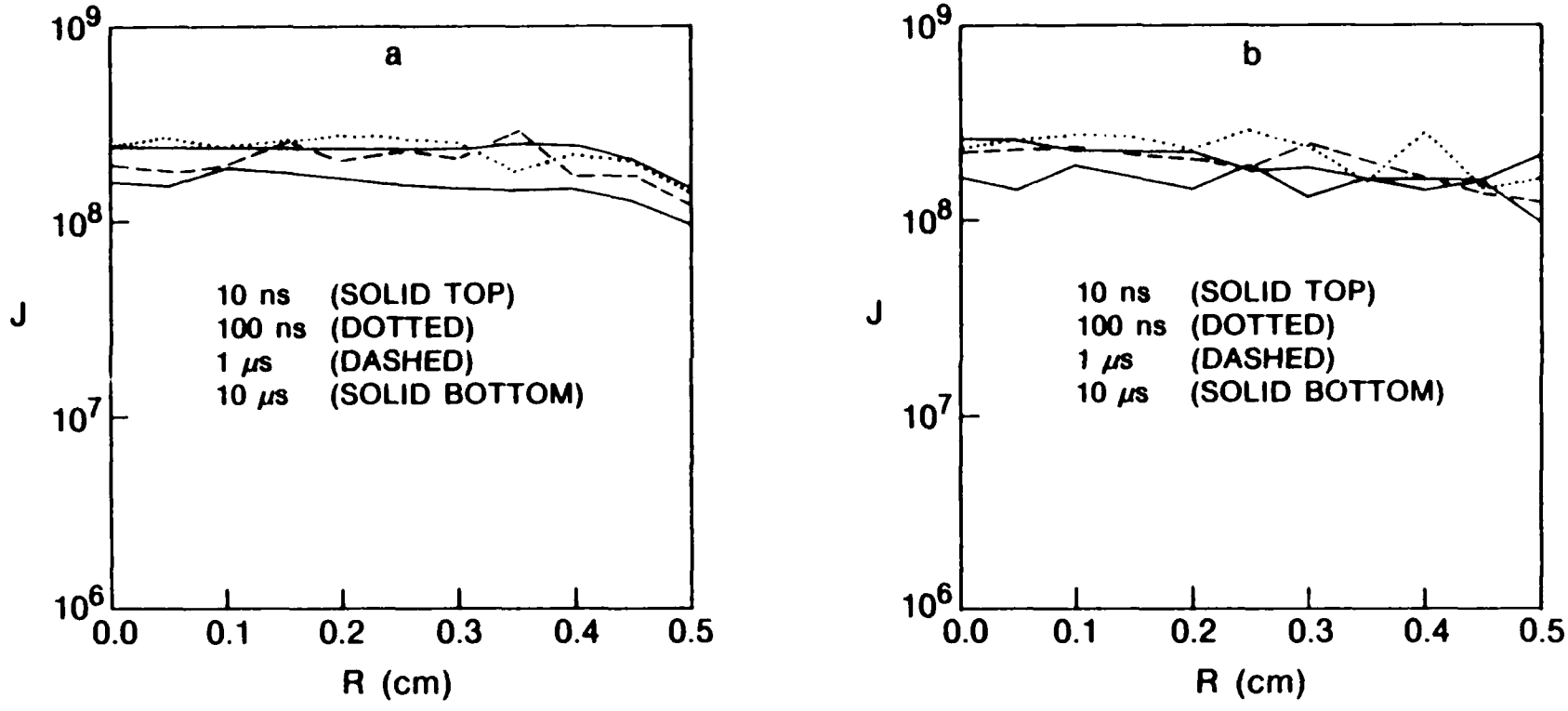

Fig. 10 Same as Fig. 9 for 8211.8 Å.

REFERENCES

1. S. Chandrasekhar, Radiative Transfer, Dover, New York (1960).

2. A. L. Crosbie and R. L. Dougherty, J. Quant. Spectrosc. Radiat. Transfer 25, 551 (1981).

3. A. S. Eddington, The Internal Constitution of the Stars, Cambridge Univ. Press (1926). Also Dover, New York (1959).

4. J. L. Kulander, J. Quant. Spectrosc. Radiat. Transfer 6, 31 (1966).

5. B. Davison (with J. B. Sykes), Neutron Transport Theory, Clarendon Press, Oxford (1957).

6. M. A. Heaslet and R. F. Warming, J. Quant. Spectrosc. Radiat. Transfer 6, 751 (1966).

7. D. R. Churchill, S. A. Hagstrom, and R. K. Landshoff, J. Quant. Spectrosc. Radiat. Transfer 4, 291 (1964).

8. L. Baker, CHARTB Multigroup Transport Package", SAND-79-0386, March 1979.

9. T. Holstein, Phys. Rev. 72, 1212 (1947); 83, 1159 (1951).

10. L. M. Biberman, Pure Appl. Chem. 13, 393 (1966).

11. J. P. Apruzese, J. Davis, D. Duston, and K. G. Whitney, J. Quant. Spectrosc. Radiat. Transfer 23, 479 (1980).

12. H. W. Drawin, Z. Physik 225, 470 (1969).

13. R. D. Taylor and A. W. Ali, "Recombination and Ionization in a Nitrogen Plasma", NRL Memorandum Report 5594, (1985). (AD-A 155 426)

14. Ronald D. Taylor and A. W. Ali, J. Quant. Spectrosc. Radiat. Transfer 35, 213 (1986).

15. R. D. Taylor and A. W. Ali, "A Collisional-Radiative Model and Saha Decrements for a Nonequilibrium Oxygen Plasma", NRL Memorandum Report 5792 (1986). (AD-A168 082)

16. Ronald D. Taylor and A. W. Ali, "Saha Decrements and Collisional-Radiative Recombination and Ionization Coefficients for a Nonequilibrium Oxygen Plasma", J. Quant. Spectrosc. Radiat. Transfer V. 25, p. 213, 1986.

17. H. Griem, Plasma Spectroscopy, McGraw-Hill, New York (1964).

18. R. D. Taylor and A. W. Ali, "Total and Partial Absorption Coefficients for a Nitrogen Plasma", NRL Memorandum Report 5607 (1985). (AD-A 157 534)

19. T. R. Young, "CHEMEQ - A Subroutine for Solving Stiff Ordinary Differential Equations", NRL Memorandum Report 4091 (1980). (AD-A 083-545)

DISTRIBUTION LIST

Chief of Naval Operations
Washington, DC 20350
ATTN: Dr. C. F. Sharn (OP09873)

U. S. Army Ballistics Research Laboratory
Aberdeen Proving Ground, Maryland 21005
ATTN: Dr. Donald Eccleshall (DRXBR-BM)
Dr. Anand Prakash

Office of Under Secretary of Defense
Research and Engineering
Room 3E1034
The Pentagon
Washington, DC 20301
ATTN: Mr. John M. Bachkosky

Office of Naval Research
800 North Quincy Street
Arlington, VA 22217
ATTN: Dr. C. W. Roberson

Chief of Naval Material
Office of Naval Technology
MAT-0712, Room 503
800 North Quincy Street
Arlington, VA 22217
ATTN: Dr. Eli Zimet

Commander
Naval Sea Systems Command
PMS-405
Washington, DC 20362
ATTN: CAPT R. Topping
CDR W. Bassett

Air Force Office of Scientific Research
Physical and Geophysical Sciences
Bolling Air Froce Base
Washington, DC 20332
ATTN: CAPT Henry L. Pugh, Jr.

Department of Energy
Washington, DC 20545
ATTN: Dr. Terry F. Godlove (ER20:GTN, High Energy and Nuclear Physics)
Dr. James E. Leiss (G-256)
Mr. Gerald J. Peters (G-256)

Joint Institute for Laboratory Astrophysics
National Bureau of Standards and
University of Colorado
Boulder, CO 80309
ATTN: Dr. Arthur V. Phelps

Lawrence Berkeley Laboratory
University of California
Berkeley, CA 94720
ATTN: Dr. Edward P. Lee

Ballistic Missile Defense Advanced Technology Center
P.O. Box 1500
Huntsville, AL 35807
ATTN: Dr. M. Hawie (BMDSATC-1)

Intelcom Rad Tech.
P.O. Box 81087
San Diego, CA 92138
ATTN: Dr. W. Selph

Lawrence Livermore National Laboratory
University of California
Livermore, CA 94550
ATTN: Dr. Richard J. Briggs
Dr. Thomas Fessenden
Dr. Frank Chambers
Dr. James W.-K. Mark, L-477
Dr. William Fawley
Dr. William Barletta
Dr. William Sharp
Dr. Daniel S. Prono
Dr. John K. Boyd
Dr. Kenneth W. Struve
Dr. John Clark
Dr. George J. Caporaso
Dr. William E. Martin
Dr. Donald Prosnitz
Dr. S. Yu

Mission Research Corporation
735 State Street
Santa Barbara, CA 93102
ATTN: Dr. C. Longmire
Dr. N. Carron

National Bureau of Standards
Gaithersburg, MD 20760
ATTN: Dr. Mark Wilson

Science Applications, Inc.
1200 Prospect Street
La Jolla, CA 92037
ATTN: Dr. M. P. Fricke
Dr. W. A. Woolson

Science Applications, Inc.
5 Palo Alto Square, Suite 200
Palo Alto, CA 94304
ATTN: Dr. R. R. Johnston
Dr. Leon Feinstein
Dr. Douglas Keeley

Science Applications, Inc.
1651 Old Meadow Road
McLean, VA 22101
ATTN: Mr. W. Chadsey

Naval Surface Weapons Center
White Oak Laboratory
Silver Spring, MD 20910
ATTN: Mr. R. J. Biegalski
Dr. R. Cawley
Dr. J. W. Forbes
Dr. D. L. Love
Dr. C. M. Huddleston
Dr. G. E. Hudson
Mr. W. M. Hinckley
Mr. N. E. Scofield
Dr. E. C. Whitman
Dr. M. H. Cha
Dr. H. S. Uhm
Dr. R. Fiorito
Dr. H. C. Chen

C. S. Draper Laboratories
Cambridge, MA 02139
ATTN: Dr. E. Olsson
Dr. L. Matson

Physcal Dynamics, Inc.
P.O. Box 1883
La Jolla, CA 92038
ATTN: Dr. K. Brueckner

Avco Everett Research Laboratory
2385 Revere Beach Pkwy
Everett, MA 02149
ATTN: Dr. R. Patrick
Dr. Dennis Reilly
Dr. D. H. Douglas-Hamilton

Defense Technical Information Center
Cameron Station
5010 Duke Street
Alexandria, VA 22314 (2 copies)

Naval Research Laboratory
Washington, DC 20375
ATTN: M. Lampe - Code 4792
M. Friedman - Code 4700.1
J. R. Greig - Code 4763
I. M. Vitkovitsky - Code 4701
J. B. Aviles - Code 6650
M. Haftel - Code 6651
T. Coffey - Code 1001
S. Ossakow - Code 4700 (26 copies)
P. Sprangle - Code 4790
Code 2628 - 20 copies
A. W. Ali - Code 4700.1 (30 copies)
D. Book - Code 4040
J. Boris - Code 4040
R. Hubbard - Code 4790
B. Hui - Code 4790
S. Slinker - Code 4790
G. Joyce - Code 4790
D. Murphy - Code 4763
A. Robson - Code 4760
D. Colombant - Code 4790
M. Picone - Code 4040
M. Raleigh - Code 4763
R. Pechacek - Code 4763
G. Cooperstein - Code 4770
Y. Lau - Code 4790
R. Fernsler - Code 4790
Code 1220 - 1 copy
Records - 1 copy

Defense Advanced Research Projects Agency
1400 Wilson Blvd.
Arlington, VA 22209
ATTN: Dr. S. Shey

Physics International, Inc.
2700 Merced Street
San Leanadro, CA 94577
ATTN: Dr. E. Goldman
Dr. H. L. Buchanon

SDIO - DEW
Office of Secretary of Defense
Washington, DC 20301
ATTN: Lt. Col. R. L. Gullickson

Mission Research Corp.
1720 Randolph Road, S.E.
Albuquerque, NM 87106
ATTN: Dr. Brendan Godfrey
Dr. Richard Adler
Dr. Thomas Hughes
Dr. Lawrence Wright

Director of Research
U.S. Naval Academy
Annapolis, MD 21402 - 2 copies

Princeton University
Plasma Physics Laboratory
Princeton, NJ 08540
ATTN: Dr. Francis Perkins, Jr.

McDonnell Douglas Research Laboratories
Dept. 223, Bldg. 33, Level 45
Box 516
St. Louis, MO 63166
ATTN: Dr. Evan Rose
Dr. Carl Leader

Cornell University
Ithaca, NY 14853
ATTN: Prof. David Hammer

Sandia National Laboratory
Albuquerque, NM 87115
ATTN: Dr. Bruce Miller
Dr. Barbara Epstein
Dr. John Freeman
Dr. John E. Brandenburg
Dr. Gordon T. Leifeste
Dr. Carl A. Ekdahl, Jr.
Dr. Gerald N. Hays
Dr. James Chang
Dr. Michael G. Mazerakis

University of California
Physics Department
Irvine, CA 92664
ATTN: Dr. Gregory Benford

Air Force Weapons Laboratory
Kirtland Air Force Base
Albuquerque, NM 87117
ATTN: D. Straw (AFWL/NTYP)
C. Clark (AFWL/NTYP)
W. Baker (AFWL/NTYP)
D. Dietz (AFWL/NTYP)
Lt Col J. Head

Pulse Sciences, Inc.
14796 Wicks Blvd.
San Leandro, CA 94577
ATTN: Dr. Sidney Putnam
Dr. John Bayless

Los Alamos National Scientific Laboratory
P.O. Box 1663
Los Alamos, NM 87545
ATTN: Dr. L. Thode
Dr. A. B. Newberger, X-3, MS-608
Dr. M. A. Mostrom, MS-608
Dr. T. P. Starke, MS-942
Dr. H. Dogliani, MS-5000

Institute for Fusion Studies
University of Texas at Austin
RLM 11.218
Austin, TX 78712
ATTN: Prof. Marshall N. Rosenbluth

University of Michigan
Dept. of Nuclear Engineering
Ann Arbor, MI 48109
ATTN: Prof. Terry Kammash
Prof. R. Gilgenbach

Directed Technologies, Inc.
226 Potomac School Road
McLean, VA 22101
ATTN: Dr. Ira F. Kuhn
Dr. Nancy Chesser

Titan Systems, Inc.
8950 Villa La Jolla Drive-Suite 2232
La Jolla, CA 92037
ATTN: Dr. R. M. Dowe

Lockheed Palo Alto Laboratory
3251 Hanover Street
Bldg. 203, Dept. 52-11
Palo Alto, CA 94304
ATTN: Dr. John Siambis

University of Maryland
Physics Department
College Park, MD 20742
ATTn: Dr. Y. C. Lee
Dr. C. Grebogi

Science Applications, Inc.
1710 Goodridge Dr.
McLean, VA 22102
ATTN: Dr. A. Drobot
Dr. K. Papadopoulos

Dr. Jonn P. Jackson
Kaman Sciences
1500 Garden of the Gods Road
Colorado Springs, CO 80933

DASIAC - DETIR
Kaman Tempo
25600 Huntington Avenue, Suite 500
Alexandria, VA 22303
ATTN: Mr. F. Wimenitz